Geoscience Frontiers 9 (2018) 1711–1724

HOSTED BY

Contents lists available at ScienceDirect

China University of Geosciences (Beijing)

Geoscience Frontiers

journal homepage: www.elsevier.com/locate/gsf

Research Paper

Geochronology and geochemistry of mafic dykes in the Helanshan complex: Implications for Mesozoic tectonics in the North China Craton

Zhenghui Li [a], Xiaoming Liu [a,*], Yunpeng Dong [a,b], M. Santosh [a,c,d], Feifei Zhang [a], Jie Xu [a]

[a] State Key Laboratory of Continental Dynamics, Department of Geology, Northwest University, Northern Taibai Road 229, Xi'an 710069, China
[b] Department of Earth Sciences, Western University, 1151 Richmond Street N. London, Ontario, N6A 5B7, Canada
[c] School of Earth Sciences and Resources, China University of Geosciences (Beijing), Beijing 100083, China
[d] Department of Earth Sciences, University of Adelaide, Adelaide 5005, Australia

ARTICLE INFO

Article history:
Received 3 June 2017
Received in revised form
4 September 2017
Accepted 25 September 2017
Available online 16 October 2017
Handling Editor: Wenjiao Xiao

Keywords:
Mafic dykes
Geochemistry
Zircon U–Pb geochronology
Hf isotope
Helanshan Tectonic Belt
North China Craton

ABSTRACT

The Helanshan tectonic belt (HTB) is a major tectonic divide between the Alxa and Ordos blocks in the North China Craton. The geochronology and petrogenesis of the mafic dykes in the northern HTB are keys to understanding the tectonic evolution of this belt. The mafic dykes, intruded into the Neoarchean–Paleoproterozoic metamorphic basement, are mainly composed of diabase with a mineral assemblage of plagioclase (45%–60%), pyroxene (25%–35%), minor quartz and Fe–Ti oxides. The LA-ICPMS U–Pb analysis of zircon grains from representative dykes yield a weighted mean age of 206 ± 1.9 Ma, which represents the crystallization age of the dyke. The diabases show high contents of $Fe_2O_3^T$ (11.88–17.55 wt.%), low contents of SiO_2 (45.65–50.95 wt.%) and MgO (3.31–5.50 wt.%) with low Mg# (=100 × MgO/(MgO + FeO) atomic ration) of 33–44. They are characterized by enrichment of light rare earth elements (LREEs) and large ion lithophile elements (LILEs) (e.g., Rb, Ba and Pb), and slight depletion of high field strength elements (HFSEs). These features suggest that the magma has undergone extensive fractionation of olivine and pyroxene but only minor crustal contamination during its evolution. Their high Sm contents and La/Sm ratios, and low Sm/Yb ratios indicate that magma from which the dykes formed was derived from low degree (about 5%) partial melting of an enriched garnet + spinel lherzolite mantle source. Together with regional geology, these geochemical and geochronological data suggest that the mafic dykes in the HTB were formed in an intracontinental extensional setting during the late Triassic.

1. Introduction

The North China Craton (NCC) has been proposed to have formed by the amalgamation of the Eastern Block, Central (Ordos) Block and the Western (Alxa) Block along the Trans-North China Orogen and the Helanshan Tectonic Belt (HTB), respectively (Zhao and Zhai, 2013) (Fig. 1). The HTB, located between the Alxa and Ordos Blocks (Fig. 2), is mainly composed of Neoarchean–Paleoproterozoic metamorphic basement rocks, and Paleoproterozoic granitoid intrusions, which are overlain by highly deformed Carboniferous–Jurassic sedimentary successions, constituting a mountain range extending from southwest to northeast. Therefore, the formation and evolutionary history of the HTB are keys to understand the tectonic evolution of the NCC, as well as the relationship between the Ordos and Alxa blocks. During the past decades, many studies have been conducted on the tectonic evolution of the HTB (Zhang et al., 2004, 2011, 2012, 2015, 2016; Dong et al., 2007; Ding et al., 2009; Xiao et al., 2011; Yin et al., 2011; Dan et al., 2012, 2014; Li et al., 2012; Yuan and Yang, 2012, 2015a,b; Xu et al., 2015), revealing the complex tectonic evolutionary history of the HTB (Lin et al., 1995) with multi-stage tectonic activities, especially during the Mesozoic (Zhang et al., 2004). The timing and tectonic correlation of the Alxa and Ordos Blocks are still controversial, although most authors argued an amalgamation along the HTB. Some workers consider the timing as Archean to Paleoproterozoic (Gong et al., 2016), whereas others propose a Phanerozoic assembly (Dan et al., 2016). For instance, a collision belt with a

* Corresponding author.
E-mail address: xmliu@nwu.edu.cn (X. Liu).
Peer-review under responsibility of China University of Geosciences (Beijing).

https://doi.org/10.1016/j.gsf.2017.09.006

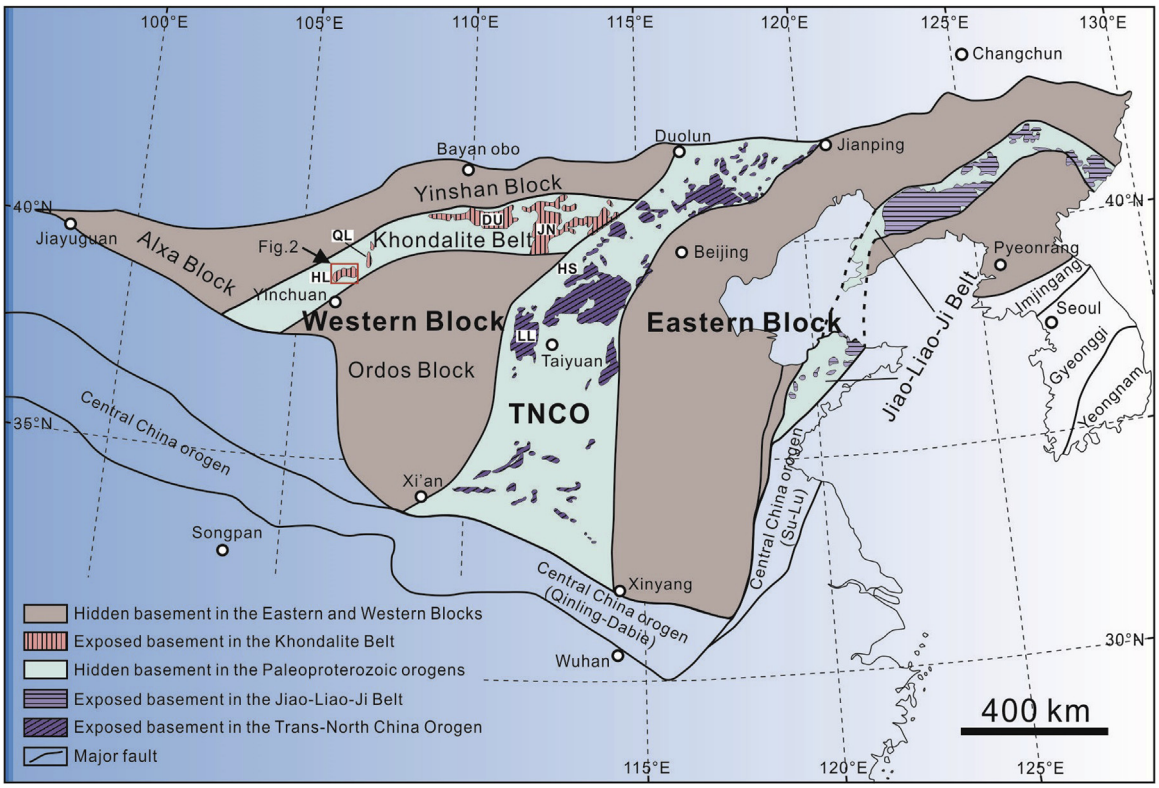

Figure 1. Simplified tectonic map showing subdivisions of the North China Craton (modified from Zhao et al., 2005). Abbreviations of metamorphic complexes: JN, Jining; DU, Daqingshan–Ulashan; QL, Qianlishan; HL, Helanshan; HS, Hengshan; LL, Lüliang; TNCO, Trans-North China Orogen.

foreland basin (Li et al., 1995; Chen, 1999; Jia et al., 2003, 2005) between the Ordos and Alxa blocks is proposed to have formed along the HTB before the Early Cretaceous (Yang et al., 2014; Yuan and Yang, 2015a) or Mid-Late Triassic (Ge et al., 2009). Other authors favor a Mesozoic intraplate extensional model (Ritts et al., 2004) or Late Triassic rift, according to the sedimentary records (Liu, 1998; Liu et al., 2013) and the geochemistry of the Rujigou basalts (Gao et al., 2003; Wang et al., 2005, 2006; Yang et al., 2010). An East Gondwana affinity has also been proposed for the western margin of the NCC during Ordovician (Wang et al., 2016). Additionally, a pull-apart basin along with strike-slip faults has also been proposed for the HTB (Zhang et al., 2009).

Detailed geological mapping has revealed the presence of many mafic dykes intruding into the basement rocks in the northern HTB (Bureau of Geological and Mineral Resources of Ningxia Hui Autonomous Region (BGMRNHAR), 1990), which serve as important indicators for the tectonic setting of the HTB. In this paper, we present results from U–Pb ages and trace element chemistry of zircon grains together with whole rock geochemical data on the representative samples of the mafic dykes from the Zongbieli and Xiaosongshan areas. Based on the results, we evaluate the timing and nature of the magma source, as well as the petrogenesis and tectonic setting of the mafic dykes. Our study provides new insights into the Mesozoic tectonics in the HTB between the Ordos and Alxa blocks.

2. Geological setting

The HTB, extending from south to north separates the Ordos Block to the east from the Alxa Block to the west, is bound by the Xiaosongshan-Alashanzuoqi-Balunbieli fault (XABF) on the west and the Shizuishan-Yinchuan fault (SYF) on the east (Fig. 2). In the southernmost part, the HTB is overthrust by the Liupanshan thrust belt along the Qingtongxia-Guyuan fault (QGF) (Fig. 2). According to the geological and structural features, the HTB can be divided into the northern, middle and southern domains by the Zhengyiguan fault (ZF) and Tujingzi-Qingtongxia fault (TQF), respectively (Zhang et al., 2004).

The northern HTB is characterized predominantly by exposures of rocks belonging to the Helanshan Complex which are composed of high grade metamorphic basement rocks, represented mainly by khondalites (Lu et al., 1996) and orthogneisses (BGMRNXHAR, 1990; Geng et al., 2009). The khondalites consist of Al-rich gneiss/granulite, quartzite, marble and calc-silicate rock (Lu et al., 1996; Yin et al., 2011), which were deposited during ca. 2.0–1.95 Ga (Zhao, 2009; Xiao et al., 2011; Yin et al., 2011; Dan et al., 2012) and underwent granulite-facies metamorphism at ca. 1.95–1.85 Ga (Dong et al., 2007; Zhao et al., 2010; Zhou et al., 2010; Yin et al., 2011). The protolith of the orthogneiss are mainly composed of biotite granite, garnet granite and TTG (tonalite-trondhjemite-granodiorite) rocks with formation ages of ca. 2.05–1.95 Ga (Geng et al., 2009; Huang et al., 2013; Li et al., 2013; Dan et al., 2014). Some Early Paleozoic carbonates, Carboniferous carbonate and clastic rocks, and Permian clastic rocks are distributed in the eastern part of the northern HTB (Fig. 2).

The middle HTB is mainly composed of Permian, Triassic and Jurassic terrestrial successions, which show unconformable contact (Ritts et al., 2004). The Permian strata consists mainly of sandstones interlayered with coal bed in the lower part, which is unconformably covered by the Middle Triassic Zhifang Formation and Upper Triassic Yanchang Formation. The Zhifang Formation mainly consists of quartz-feldspar sandstones interlayered with thin-layered siltstones, whereas the Yanchang Formation is characterized by thick-layered quartz-feldspar sandstones interlayered with gray-black muddy siltstones and shales (BGMRNXHAR,

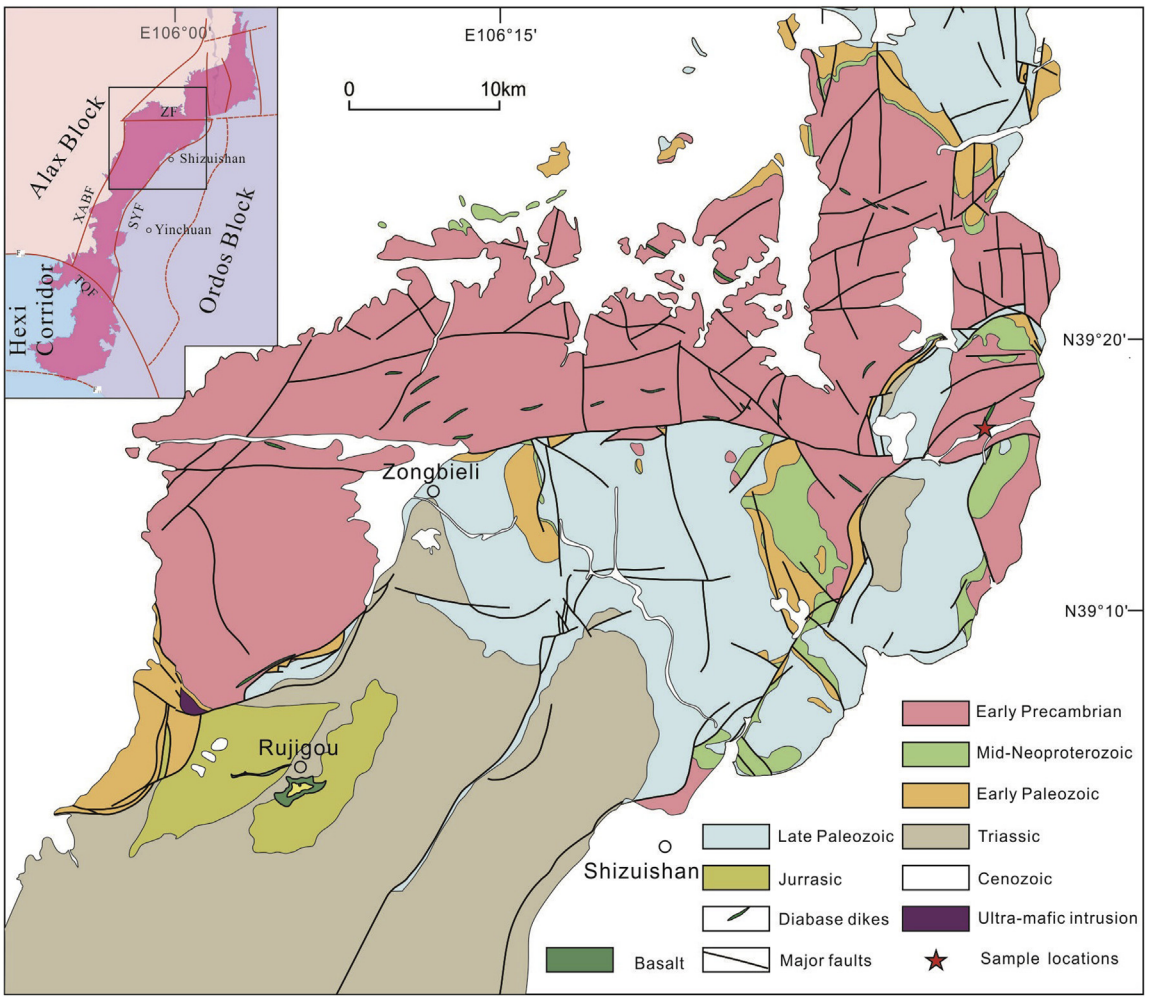

Figure 2. Geological map of the study area in the Helanshan (modified from the 1:200,000 geological maps). Abbreviations: ZF, Zhengyiguan fault; TQF, Tujingzi–Qingtongxia fault; XABF, Xiaosongshan–Alashanzuoqi–Balunbieli fault; SYF, Shizuishan–Yinchuan fault.

1990). These sedimentary features reflect fluvial, lacustrine-deltaic and alluvial fan tectonic setting and evolutionary processes (Ritts et al., 2004). The Jurassic sandstones, mudstones and interlayered coals unconformably lie over the Triassic sandstones, and were occasionally covered by the lower Cretaceous coarse-grained sandstones (BGMRNXHAR, 1990). A few basement rocks are exposed in the northernmost domain of the middle HTB (Fig. 2).

The southern HTB is characterized mainly by voluminous Early Paleozoic fine-grained clastic rocks, Devonian molasses and minor Triassic and Jurassic terrestrial clastic rocks (Huo et al., 1989; Zhang, 1989).

According to the lithological association, deformation and metamorphism, the northern, middle and southern HTB are considered to expose the uppermost crust from lower to upper parts. The lower part is featured by basement rock with mafic dykes, whereas the middle part is mostly cover sequences with basaltic lavas. For example, the basalts exposed at Rujigou in the middle HTB with low-K tholeiitic compositions (Wang et al., 2006) might represent the eruption and shallow chamber of a mafic magma, whereas the mafic dykes in the northern HTB represent the lower and intrusive member of the mafic magma. A K–Ar age of 229 ± 15 Ma has been reported (BGMRNXHAR, 1990), together with the basalt overlying the Upper Triassic strata, which indicates that the formation age of the basalt is not earlier than the Late Triassic.

3. Sample description

The mafic dykes mostly intrude into the high-grade basement rocks comprising khondalites and orthogneisses in the northern HTB. The representative samples of the mafic dyke swarms for this study were collected from the northern HTB (N39°17′062″ and E106°39′001″) (Fig. 2). The dykes are commonly 2–3 km long and up to 10 m wide (Figs. 2 and 3a), and are characterized by fine-grained texture with 3–5 cm wide chilled margins. The dykes show typical diabasic texture (Fig. 3c and d), and consist mainly of clinopyroxene (25%–35%) and plagioclase (45%–60%) with chlorite and epidote (~5%), Fe–Ti oxides (~5%) and accessory minerals (~5%). The plagioclase occurs as subhedral to anhedral crystals (0.2–0.4 mm). Some grains of clinopyroxene and plagioclase were partly replaced by chlorite during the weak low-temperature alteration. Small crystals of Fe–Ti oxides are widely disseminated in the samples, and trace amounts of zircon are also present.

Fourteen representative samples were selected for whole-rock geochemical analysis, and one of these was chosen for zircon U–Pb dating and Hf isotope analysis. All these analyses were

Figure 3. (a) Outcrop photograph showing a mafic dyke intruding the granite in the Helanshan. (b) Outcrop photograph showing fresh surface and massive structure of the mafic dyke. (c) and (d) Photomicrograph of the mafic dyke. Cpx, Clinopyroxene; Pl, Plagioclase.

carried out at the State Key Laboratory of Continental Dynamics, Northwest University, China.

4. Analytical methods

4.1. LA-ICP-MS zircon U–Pb dating

Zircon grains were concentrated by means of a Wilfley table using conventional heavy liquid and magnetic techniques. The zircon grains were handpicked under a binocular microscope and mounted on a disc of 20 mm in diameter with epoxy resin. The mount was polished until the zircon interiors were exposed. The internal and external textures of the zircon grains were observed using transmitted and reflected light. The cathodoluminescence (CL) images were taken using FEI Qunta 400 FEG SEM equipped with MONO CL3 + Fluorescence Spectrometer, and the images were used to identify the internal texture and to select optimum spot locations for U–Pb dating. Zircon grains were dated in-situ on the LA-ICP-MS. Prior to zircon U–Pb dating, the grain surfaces were washed in dilute HNO_3 and pure alcohol to remove any potential lead contamination. The zircon U–Pb analyses were conducted on an Agilent 7500a ICP-MS equipped with a 193 nm ArF-excimer laser (MicroLas Pro). A 32 μm spot diameter was utilized in this study with a laser repetition rate of 6 Hz. The Harvard zircon 91500 was used as an external reference (recommended $^{206}Pb/^{238}U$ age of 1065.4 ± 0.6 Ma) (Wiedenbeck et al., 2004) to correct both instrumental mass bias and depth-dependent elemental and isotopic fractionation. The raw data were processed using the GLITTER 4.0 (Macquarie University) to calculate the ratios of $^{207}Pb/^{206}Pb$, $^{206}Pb/^{238}U$, $^{207}Pb/^{235}U$ and $^{208}Pb/^{232}Th$. The ages were calculated using ISOPLOT programs (Ludwig, 2003). The NIST610 was used as an external reference and Si as internal standard in calibrating trace element contents. The analytical details were described by Liu et al. (2007).

4.2. Zircon Lu–Hf isotope analyses

In situ zircon Hf isotope analyses were performed on a Nu Plasma II MC-ICP-MS (Nu Instruments Ltd., UK) equipped with a Resolution M50 excimer ArF laser-ablation system at the State Key Laboratory of Continental Dynamics, Northwest University, Xi'an, China. A 4 Hz repetition rate and 43 μm spot size were used during laser ablation. To monitor data quality, 91500 and Mud Tank were reanalyzed as unknown samples, and the obtained $^{176}Hf/^{177}Hf$ ratios were 0.282309 ± 0.000020 (n = 10, 2σ) for 91500 and 0.282521 ± 0.000024 (n = 5, 2σ) for Mud Tank. These results agree well with the recommended $^{176}Hf/^{177}Hf$ ratios 0.282330 ± 0.000029 (2σ) for 91500 and 0.282523 ± 0.000043 (2σ) for Mud Tank within 2σ (Griffin et al., 2006). Data processing was based on a decay constant for ^{176}Lu (1.867×10^{-11} yr^{-1}) (Albarède et al., 2006) and the present-day chondritic ratios of $^{176}Hf/^{177}Hf$ (0.282772) and $^{176}Lu/^{177}Hf$ (0.0332) (BlichertToft and Albarede, 1997) for the calculation of ε_{Hf}. Single stage model ages (T_{DM}) were calculated by reference to depleted mantle with the present-day $^{176}Hf/^{177}Hf$ ratio (0.28325) and $^{176}Lu/^{177}Hf$ ratio (0.0384) (Griffin et al., 2000). The two-stage model ages (T_{DM}^{c}) were calculated by projecting the initial $^{176}Hf/^{177}Hf$ of zircons back to the depleted mantle growth curve using a value of $^{176}Lu/^{177}Hf$ = 0.015 for average continental crust

(Rudnick and Gao, 2003). Detailed analytical procedures were similar to those described by Yuan et al. (2008).

4.3. Whole-rock geochemical analyses

Altered surfaces were carefully removed from all the selected samples and the rocks were washed and crushed to about 60 meshes in a WC jaw crusher (Restch BB200 WC). About 100 g of the sample was powdered in a WC Mill (Retsch, RS200) to less than 200 meshes (75 μm) for whole rock analysis. For major element analysis, 0.700 g sample powders were mixed with 3.60 g $Li_2B_4O_7$, 0.30 g LiF, 0.40 g NH_4NO_3 and 2–3 drops 1.5% (w/w) LiBr solution. The mixture was put into a platinum (Pt 95% + Au 5%) crucible, and melted in a high frequency melting instrument into a glass disks prior to analysis. The glass disks were analyzed by XRF (Rigaku RIX2100). For trace elements analysis, 50.00 mg sample powders were digested using HNO_3, HF and $HClO_4$ in polytetrafluoroethylene (PTFE) bombs with steel sleeves heated in an electronic oven at 190 °C for 48 h. The detailed sample preparation procedure followed those in Liu et al. (2014). The final solutions, diluted to 80.00 g using 2% HNO_3 with internal standard (10 ng/g Rh in the solution), were analyzed using ICP-MS (Agilent 7500a). Analysis of USGS rock standards (BCR-2, BHVO-1 and AVG-1) indicate that the precision and accuracy are better than 5% for major elements and 10% for trace elements.

5. Results

5.1. U–Pb ages and trace element composition of zircons

More than two hundred zircon grains were concentrated from the sample 15HL-28 (>65 kg) which was collected from a 40 m wide mafic dyke. All the zircon grains from the diabase dykes can be divided into two groups based on color and shape (Fig. 4). The first group exhibits well-developed crystal faces with length/width ratios ranging from 2:1 to 5:1 and show bright color with magmatic zoning in the rims, suggesting magmatic origin (Fig. 4a). The second group is characterized by dark-color and length/width ratios of 1:1 to 2:1. The optical and cathodoluminescence (CL) images show that these zircon grains are predominantly homogeneous, opaque to translucent at the rims, with slight magmatic oscillatory zoning in the cores (Fig. 4b–d). These features suggest that the second group zircons are evolved magmatic grains captured by the dykes.

One hundred and thirty two spots were analyzed from 128 zircon grains (Fig. 5a). The analytical results of U–Pb are listed in Supplementary Table 1. All zircon U–Pb data are plotted on $^{207}Pb/^{235}U$–$^{206}Pb/^{238}U$ concordia diagram (Fig. 5a), and the results show different degrees of isotopic resetting. The concordant ages (degree of concordance between 95% and 105% of $^{207}Pb/^{235}U$ relative to $^{206}Pb/^{238}U$ for age <1.0 Ga and $^{206}Pb/^{238}U$ relative to $^{207}Pb/^{206}Pb$ for age >1.0 Ga zircons), were plotted in Fig. 5b. The inset is the relative probability plot. The data show that the concordant zircon grains belong to distinct ages of 200 Ma, 800 Ma and 1.8 Ga with a few scattered ages of 1.9 Ga, 2.1 Ga, 2.3 Ga and 2.5 Ga. The discordant zircons, with $^{207}Pb/^{206}Pb$ ages of younger than 1.84 Ga, yield upper and lower intercept ages of 1818 ± 17 Ma and 207 ± 31 Ma, respectively (Fig. 5c). The concordant zircons with ages of about 1.8 Ga yield weighted mean $^{207}Pb/^{206}Pb$ age of 1816 ± 21 Ma (2σ, n = 18), which is consistent with the upper intercept age. The other seven concordant data yield a weighted mean $^{206}Pb/^{238}U$ age of 205.5 ± 1.9 Ma (2σ, n = 7) (Fig. 5d), which is similar to the lower intercept age of 207 ± 31 Ma.

The trace element contents of zircons are listed in Supplementary Table 2. The chondrite-normalized REE patterns

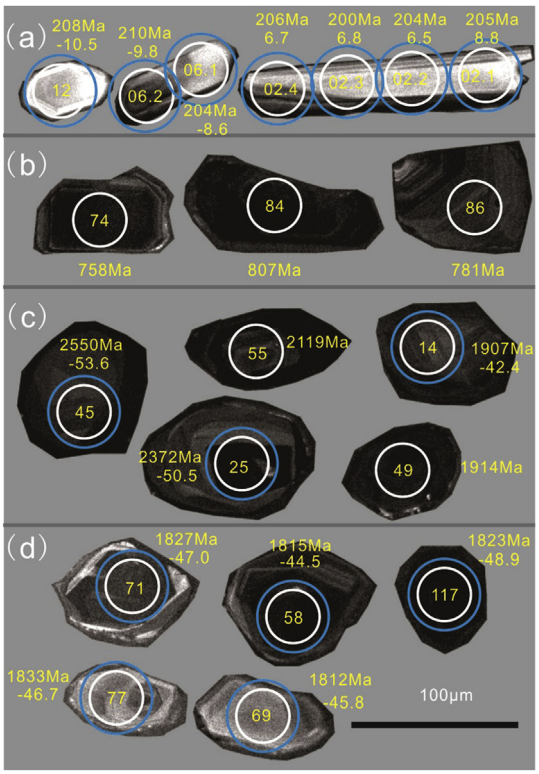

Figure 4. Representative cathodoluminescence (CL) images of zircon grains from the sample. White circles denote U–Pb dating spots (32 μm) and blue circles show Lu–Hf analysis spots (43 μm).

and the variation of Th/U ratios with the U–Pb ages of concordant zircons are shown in Fig. 6a and b, respectively. All concordant zircons show LREE depletion, positive Ce anomalies and negative Eu anomalies (Fig. 6a). The Th/U ratios of all concordant zircons are larger than 0.3 except for one grain with 0.18 (1.91 Ga). Four analyses from zircon 15HL-28-02 show slight enrichment in heavy REE and negative anomalies of Eu/Eu* (>0.7) compared with the other concordant zircons (0.1–0.6) and the larger Th/U ratios of 0.58. These features suggest that zircon 15HL-28-02 may have a different origin from the other concordant zircons.

5.2. Zircon Lu–Hf isotopes

Hf isotopic analyses were conducted on the same zircon grains that were previously analyzed for U–Pb isotopes. Zircon Hf isotopic data are listed in Supplementary Table 3 and plotted in Fig. 7. Hf isotope analysis of 27 concordant zircons was undertaken for sample 15HL-28. Four analyses from zircon grain15HL-28-02 with ages of 200–206 Ma display positive $\varepsilon_{Hf}(t)$ values ranging from 10.6 to 13.0. Three analyses from two zircons with ages about 204–210 Ma have negative $\varepsilon_{Hf}(t)$ values ranging from −6.12 to −4.31 with single-stage model ages (T_{DM}) ranging from 1034 to 1105 Ma.

The old zircon grains show a range of $\varepsilon_{Hf}(t)$ values and model ages. Two grains (15HL-28-25 and 15HL-28-45) with ages of 2372 Ma and 2550 Ma show positive $\varepsilon_{Hf}(t)$ values of 1.86 and 3.14. Except for 15HL-28-98 and 15HL-28-109 which display positive $\varepsilon_{Hf}(t)$ values of 1.84 and 5.43, the other zircon grains with ages of 1781–1845 Ma have negative $\varepsilon_{Hf}(t)$ values of −4.91 to −9.31, and two-stage model ages (T_{DM}^{C}) varying from 2597 to 2812 Ma. All these data suggest these zircon grains are xenocrysts captured from country rocks.

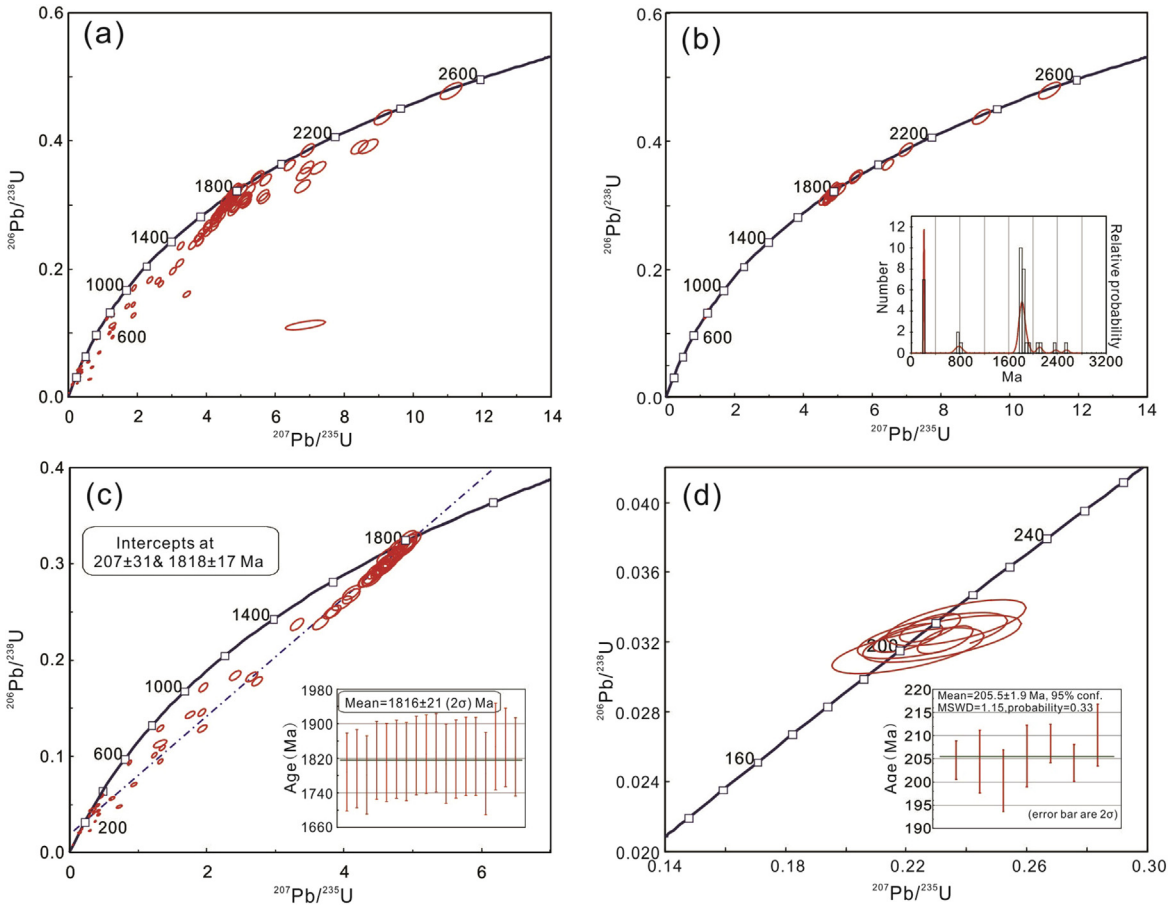

Figure 5. U–Pb concordia plots: (a) for all zircons, (b) for the zircons with concordant degree between 95% and 105% (the inset is the relative probability plot), (c) for discordant zircons with $^{207}Pb/^{206}Pb$ ages of less than 1837 Ma except for the concordant zircons with the $^{206}Pb/^{238}U$ ages of about 200 and 800 Ma (the inset is the weight mean plot of concordant zircons with ages of about 1816 Ma), and (d) for the zircons with concordant ages of 205 Ma (the inset is the weight mean plot of about 205 Ma zircons).

5.3. Major and trace elements

Whole-rock major and trace element compositions of the representative samples of mafic dykes from the northern HTB are listed in Supplementary Table 4.

The mafic dykes have low contents of SiO_2 (45.65–50.95 wt.%), MgO (3.31–5.50 wt.%) and Al_2O_3 (12.08–14.78 wt.%), and high contents of $Fe_2O_3^T$ (11.88–17.55 wt.%). Their low K_2O contents range from 1.64 to 2.63 wt.% and ($K_2O + Na_2O$) values range from 3.78 to 5.45 wt.% with K_2O/Na_2O ratios of 0.52–1.01. The rocks exhibit moderate to high loss on ignition (LOI) values (2.03–5.94 wt.%) (Supplementary Table 4), and thus the TAS diagram may be not suitable in the present case to classify the volcanic series (Fig. 8a). Nb and Y are generally considered to be immobile during alteration. Here we discriminate the mafic dykes by means of Nb/Y ratios. The mafic dykes can be classified as subalkaline basaltic rocks, as shown in Nb/Y vs. $Zr/TiO_2 \times 0.0001$ diagram (Fig. 8b). They display low Mg# values ($=100 \times MgO/(MgO + FeO)$ atomic ratio) ranging from 33 to 44, and Cr and Ni contents varying from 2.1 to 58.2 ppm and from 7.3 to 48.4 ppm, respectively. Their low Al_2O_3 and MgO

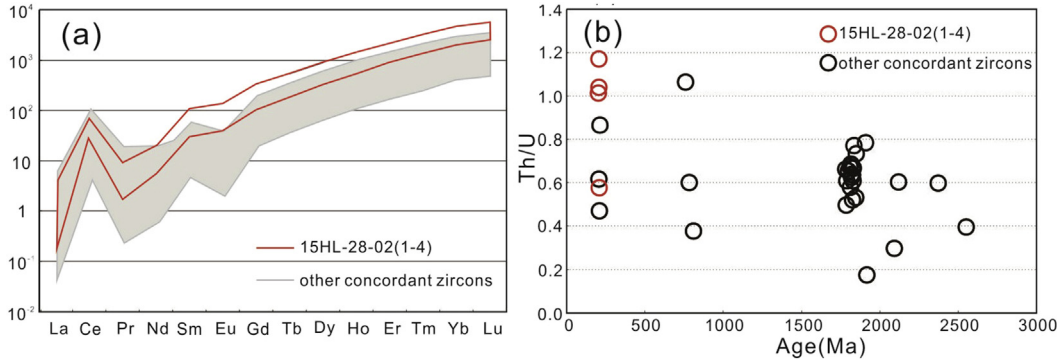

Figure 6. (a) Chondrite-normalized REE patterns of concordant zircons, closed red line showing the changes in zircon 15HL-28-02 and difference between the zircon and other concordant zircons (gray area). (b) The changes of Th/U ratios with ages of concordant zircons, red circles showing the Th/U ratios of zircon 15HL-28-02.

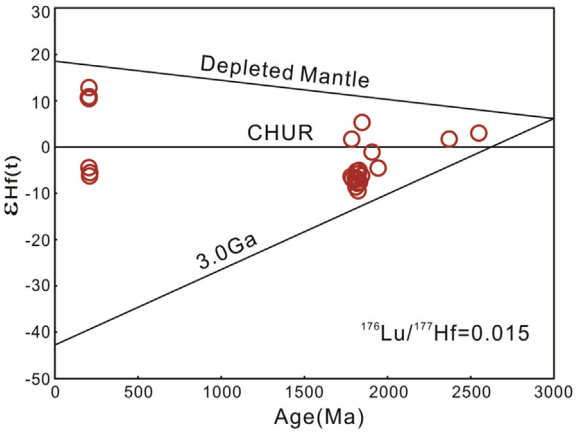

Figure 7. Plot of $\varepsilon_{Hf}(t)$ values vs. crystallization ages for the zircons from the mafic dykes in the Helanshan.

contents, and high Fe_2O_3 and TiO_2 suggest that the mafic dykes are high-Fe tholeiite (Fig. 8c).

In Harker diagrams, SiO_2, CaO, and P_2O_5 correlate negatively with MgO (Fig. 9a,e,f), and TiO_2 and $Fe_2O_3^T$ correlate positively with MgO (Fig. 9c and d), while there is no clear correlation between Al_2O_3 and MgO (Fig. 9b). Among the trace elements, Sr, Ce, Zr and Th show negative correlations with MgO (Fig. 10c–f), whereas Cr and Ni show positive correlations with MgO (Fig. 10a and b).

The chondrite-normalized rare earth element (REE) patterns (Fig. 11a) of the samples exhibit enrichment of light rare earth element (LREE) with $(La/Yb)_N$ of 4.75–7.74 and negative Eu anomalies (Eu/Eu* = 0.68–0.87). In the primitive mantle-normalized trace element spider diagrams, the samples show clear enrichment of large-ion lithophile elements (LILEs, e.g., Cs, Rb, Ba, Th, U, K and Pb, etc.), and enrichment and differentiation of high field strength elements (HFSEs) with strong negative Sr anomalies, and slightly Nb, Ta and Ti depletions (Fig. 11b).

6. Discussion

6.1. Timing on the mafic dykes

Concordant zircon grains from the studied mafic dyke display age ranges of ca. 200 Ma and 1.8 Ga, and a few scattered ages (Fig. 5). Seven concordant analyses yield a weighted mean $^{206}Pb/^{238}U$ age of 205.5 ± 1.9 Ma. These zircon grains are bright, translucent to opaque with well-developed crystal faces and slight magmatic oscillatory zoning in the rims (Fig. 4a) suggesting their magmatic affinity (Corfu et al., 2003; Wu and Zheng, 2004). This conclusion is also supported by their high Th/U ratios of 0.57–1.17 (Fig. 6b), as in general, the Th/U ratios of magmatic zircons mostly range from 0.2 to 1.0, whereas zircons crystallized during metamorphic events exhibit lower Th/U ratios (<0.1) (Williams and Claesson, 1987; Schiøtte et al., 1988; Kinny et al., 1990).

The chondrite normalized REE patterns of 4 spot analyses of zircon 15HL-28-02 show slight Eu/Eu* anomalies (0.70–0.72) relative to other concordant zircons (0.05–0.62 with average value of 0.26) (Fig. 6a). The contents of Lu, U and Ta of this zircon range from 99 to 129 ppm, 223 to 313 ppm and 1.2 to 1.5 ppm, respectively. The Hf contents of four spot analyses are 0.73%, 0.77%, 0.79% and 0.96%. These features correspond to basaltic origin with Lu > 20.7 ppm, U > 38 ppm, Ta > 0.58 ppm and Hf < 0.8% (Belousova et al., 2002). The 1.8 Ga concordant zircons show Lu > 31.8 ppm, U > 132 ppm, Ta > 1.28 ppm except for one zircon

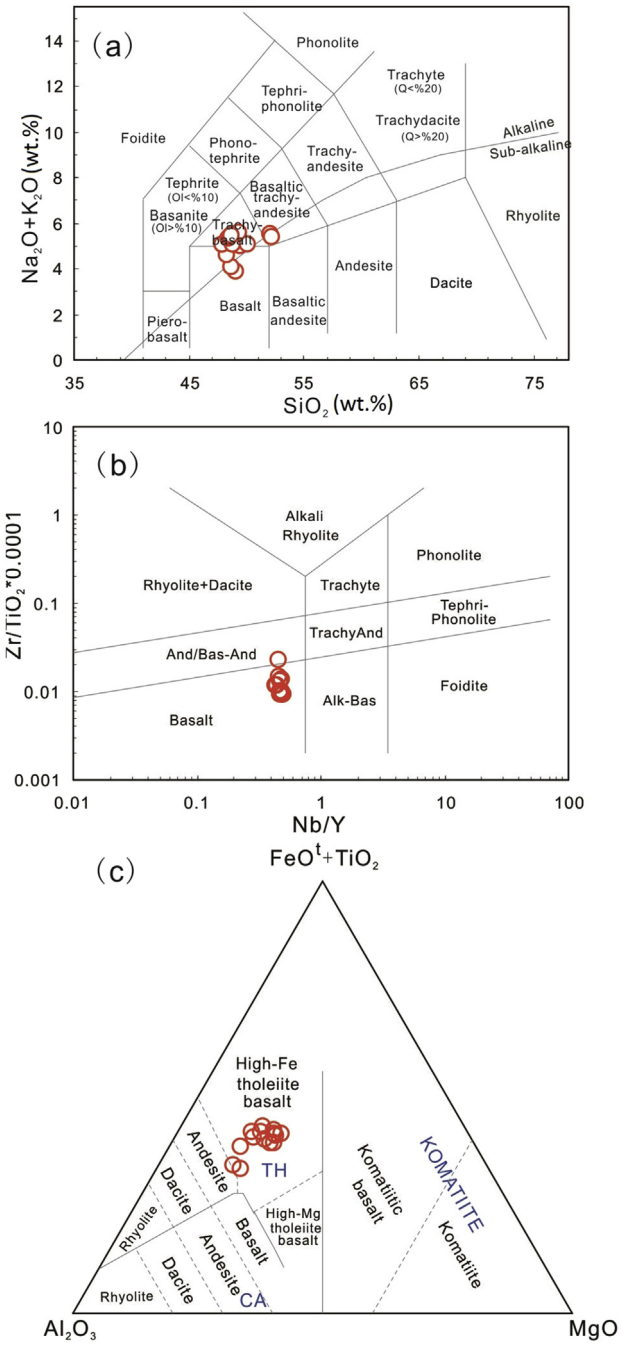

Figure 8. (a) Total alkali-silica (TAS) diagram for the mafic dykes in the Helanshan (after Le Bas et al., 1986). (b) Nb/Y–Zr/TiO_2 × 0.0001 diagram (after Winchester and Floyd, 1977). (c) Jensens cation plot (Jensen, 1976), using major element concentrations recalculated to 100% volatile-free compositions.

with 0.46 ppm and Hf > 0.83% which are characteristics of granitoid zircons (Belousova et al., 2002).

The trace element characteristics and the positive $\varepsilon_{Hf}(t)$ values of zircon 15HL-28-02 with ages of 200–206 Ma suggest that the zircon grains crystallized from a magma derived through partial melting of mantle. Therefore, the weighted mean $^{206}Pb/^{238}U$ age of 205.5 ± 1.9 Ma can be interpreted as the intrusive age of the mafic dyke. The negative $\varepsilon_{Hf}(t)$ values of other two zircons with ages of about 204–210 Ma might be related to crustal contamination. For the ca. 1.8 Ga concordant zircons, the trace element characteristics

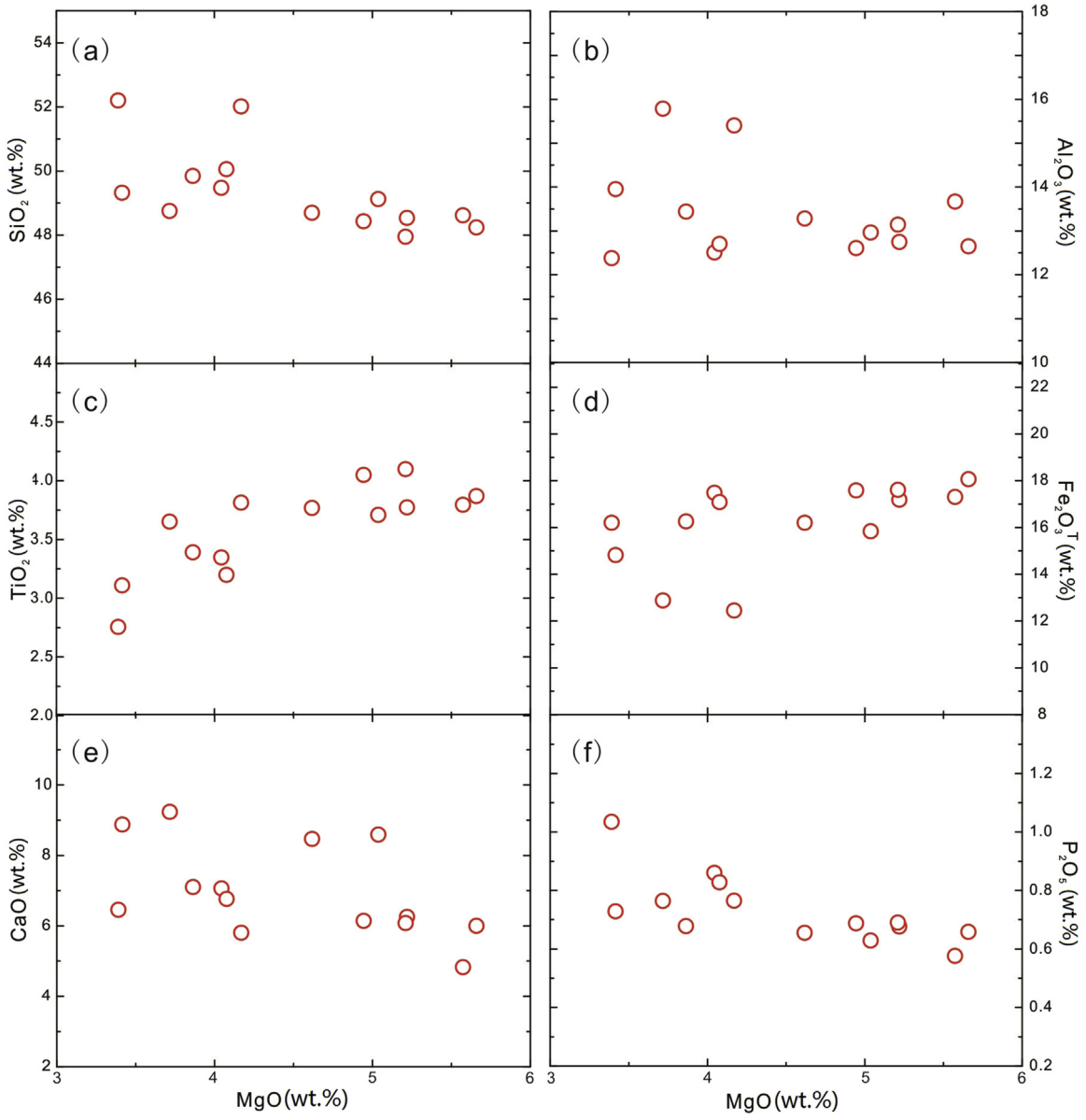

Figure 9. Harker diagrams of major elements vs. MgO for the mafic dykes in the Helanshan.

suggest their granitoid origin, and their negative $\varepsilon_{Hf}(t)$ values and two-stage model ages (T_{DM}^{C}) of 2.6–2.8 Ga imply that these zircons were crystallized from the magma originated through melting of 2.4–2.8 Ga old crust materials.

Some zircons with old ages ranging from 2.55 Ga to 758 Ma indicate that they were captured from the country rocks. According to their ages, the second group of zircons with dark color displays mainly two age spans of ca. 807–758 Ma and ca. 1.83–1.81 Ga and some grains show ages of 1.9 Ga, 2.1 Ga, 2.37 Ga and 2.55 Ga (Fig. 4b–d). The zircon grains with ages of ca 1.8 are common in the dykes, and show bright-color and magmatic oscillatory zoning in the cores (Fig. 4d), which are similar to that of zircons from granitoids. The TTG suite in the HTB was mainly formed during ca. 2.05–1.95 Ga (Geng et al., 2009; Huang et al., 2013; Li et al., 2013; Dan et al., 2014), whereas the S-type granites occurring in the central HTB display zircon ages of 1.95 Ga (Li et al., 2013) and 1.86 Ga (Yin et al., 2011). Therefore, the zircons in our samples were most likely captured from the granitoids in the basement of the HTB. The grains with ages of 2.1 Ga, 2.37 Ga and 2.55 Ga might be detrital zircons from the khondalite (Yin et al., 2011).

Three concordant zircons have ages of 758–805 Ma, and show euhedral external structure, oscillatory zoning internal texture on CL images (Fig. 4b) and high Th/U ratios (0.38–1.07) (Fig. 6b) suggesting magmatic origin. The occurrence of zircons with ages of 750–800 Ma might suggest the presence of Neoproterozoic rocks beneath the Helanshan complex.

6.2. Origin of the mafic dykes

6.2.1. Alteration effects

The mafic dykes in our study have relatively high LOI (2.03–5.94 wt.%), suggesting that these rocks might have undergone alteration. Petrographic studies reveal that some grains of the pyroxenes and plagioclases were partially replaced by chlorite and epidote. Some incompatible elements, such as Rb, Ba and K, are known to be mobile during weathering (Deniel, 1998), as

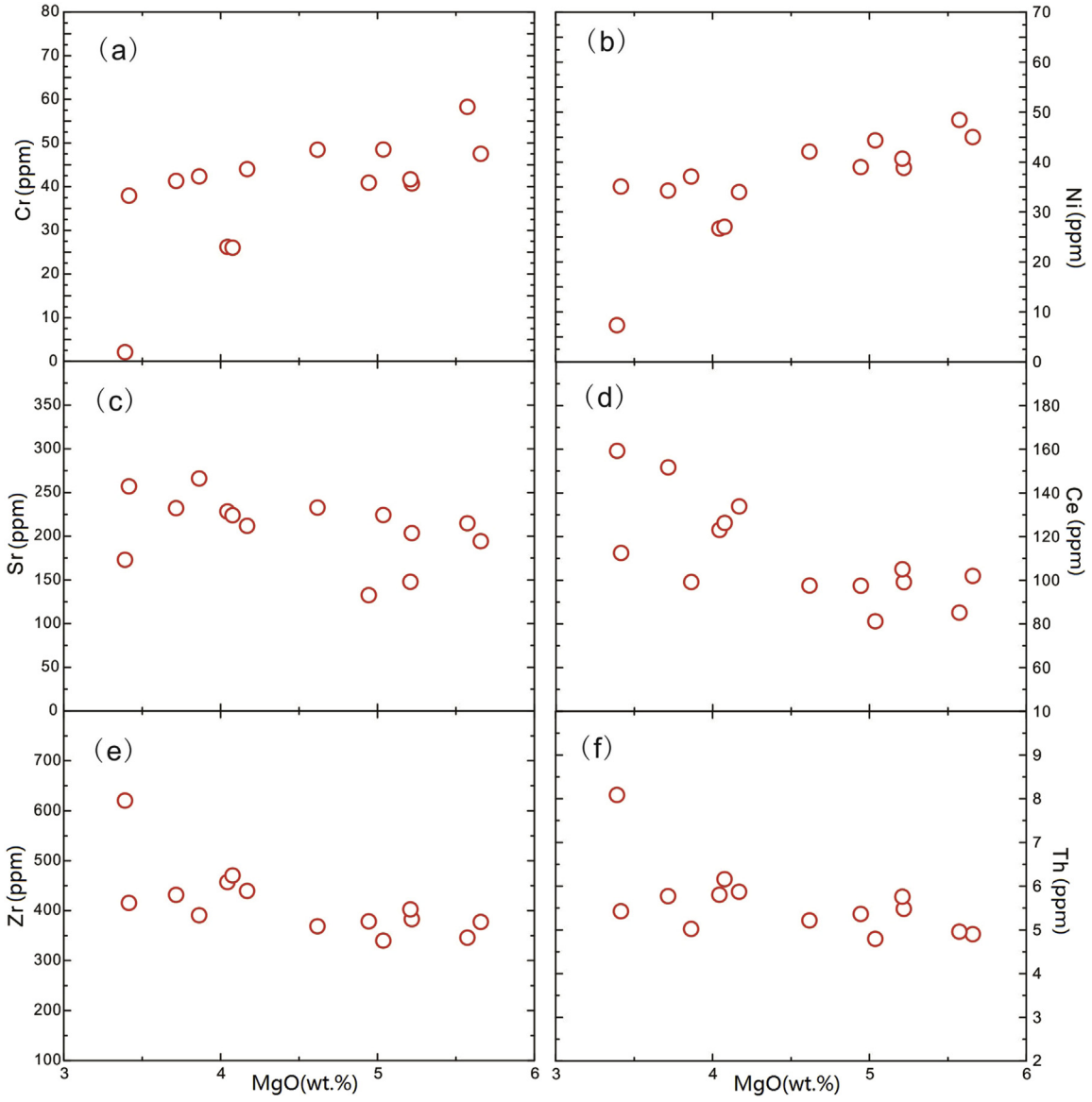

Figure 10. Harker diagrams of trace elements vs. MgO for the mafic dykes in the Helanshan.

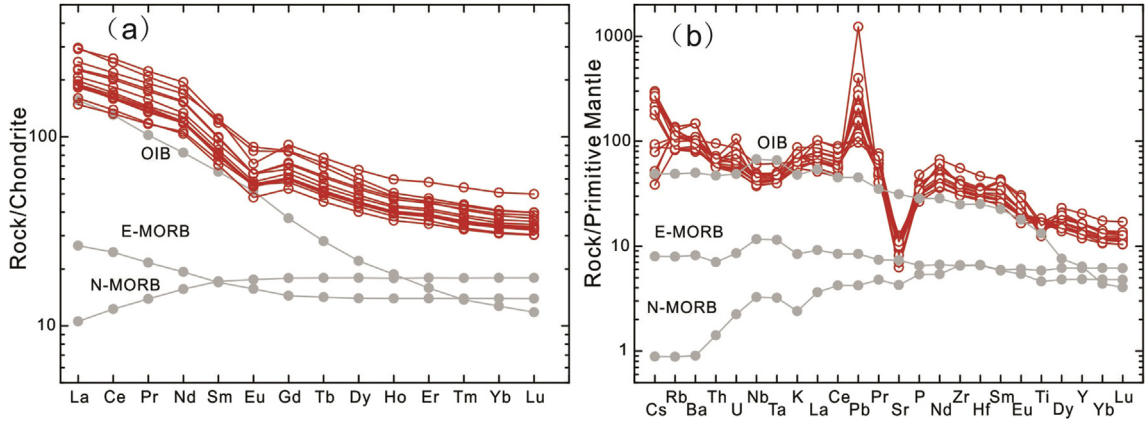

Figure 11. Chondrite-normalized REE patterns and Primitive mantle-normalized trace element patterns for the mafic dykes in the Helanshan. The values of Chondrite, Primitive Mantle, OIB, E-MORB and N-MORB are from Sun and McDonough (1989).

demonstrated by the considerable scatter shown in Fig. 11b. However, the parallel patterns of absolute abundances and ratios of incompatible elements (except for Rb, Ba and K) suggest minimal alteration of primary igneous values, as shown in Fig. 11b. This is also supported by high K, Th contents and constant K_2O/Rb ratios (219–334). Moreover, element mobility, tested by plotting major and trace element data against LOI (not shown), reveals a low degree of mobility for K, Na, Rb and Sr. Thus, we preclude significant alteration effects in the samples. Therefore, the following discussions will use these immobile elements to discuss the petrogenesis of the dykes.

6.2.2. Fractional crystallization

Low MgO content (mostly <6 wt.%), Mg# (33–44), and Ni content (7.30–48.42 ppm) indicate that the mafic dyke does not represent primary melt that was in equilibrium with mantle peridotites, implying extensive fractional crystallization of the mafic magma. As shown in the diagrams of La/Sm versus La (Fig. 12a) and Th/Hf versus Th (Fig. 12b), the samples show horizontal trends, which indicate significant fractionation processes (Allegre and Minster, 1978). Furthermore, the samples show increasing in $Fe_2O_3^T$, Cr and Ni contents with increasing MgO content (Figs. 9d and 10a, b), which indicate fractionation of olivine and clinopyroxene during the magma evolution. Positive correlations between TiO_2, $Fe_2O_3^T$ and MgO (Fig. 9c and d) suggest a certain amount of fractionation of Fe–Ti oxides crystallized from melt. Fractional crystallization of plagioclase has also played an important role in the magma evolution, as reflected in low Eu/Eu* values of 0.68–0.87 and negative Sr anomalies (Fig. 11).

6.2.3. Crustal contamination

The Archean and Paleoproterozoic ages of zircon grains in the mafic dyke provide evidence for crustal contamination, and thus it is necessary to assess the degree of crustal contamination during magma ascent. Crustal materials are enriched in LILE, Na_2O but depleted in TiO_2. The mafic dykes from HTB exhibit low Na_2O (2.11–3.38 wt.%) and high TiO_2 (2.69–3.98 wt.%) contents, suggesting minimal crustal contamination. Crustal materials are depleted in Nb and Ta but enriched in Zr and Hf, and therefore, crustal contamination might produce significant negative Nb and Ta anomalies relative to LILE and LREE but generate positive Zr and Hf anomalies (Sun and McDonough, 1989; Zhao and Zhou, 2007). The slight negative Nb–Ta and Zr–Hf anomalies observed in the primitive mantle-normalized trace element spider diagrams argue against significant crustal contamination (Fig. 11b). The studied mafic dykes have relatively higher Zr/Nb and lower Th/Nb ratios (12.38–14.44 and 0.16–0.19, respectively) than those of the OIB (4.2 and 0.66, respectively), which also suggests minor crustal contamination during their ascent. In addition, the mafic dykes show very sharp contacts and no evidence of reaction with the host granitoids in the field. Thus, significant crustal contamination during the magma ascent can be excluded. Their geochemical features can therefore provide important information about the nature of the mantle source (Fitton, 1995).

6.2.4. Nature of the mantle source

The low SiO_2 contents (45.65–50.95 wt.%) of these rocks suggest that the mafic dykes were derived from an ultramafic source and originated directly from the mantle (Liu et al., 2008, 2009). As shown above, the samples have high REE contents (231.40–426.30 ppm) and show enrichment in LREE, suggesting an enriched mantle source for the mafic dykes. Moreover, incompatible element enrichments also indicate that they likely originated from an enriched mantle.

Ratios of incompatible elements can be used to evaluate the source characteristics. The Zr/Nb ratios (12.38–14.44) of these rocks are much higher than that of OIB (5.83), which suggests that they are not derived from an OIB-like asthenosphere mantle. The sample with lower $(Nb/La)_{PM}$ (0.44–0.75 less than 1) could be ascribed to either crustal contamination or the involvement of a lithospheric mantle component. As mentioned above, crustal contamination en route was negligible through the crust. Therefore, the magma of the mafic dykes likely originated from a lithospheric mantle component involved source.

The composition of the mantle source and degree of partial melting can be determined using REE abundances and ratios. Partial melting of a spinel-lherzolite mantle source would decrease La/Sm ratios and Sm contents of the melts (Aldanmaz et al., 2000), but may not change Sm/Yb ratio because Sm and Yb have similar partition coefficients (Dong et al., 2017). This would define melting trends sub-parallel to the mantle array, whereas the partial melting of garnet-lherzolite would result in steep melting trends (Zhao and Zhou, 2007). In the Sm/Yb vs. Sm (Fig. 13a) and Sm/Yb vs. La/Sm diagrams (Fig. 13b), the Sm/Yb ratios of the mafic dykes are higher than those of typical spinel lherzolite, but lower than those of the garnet-lherzolite, and they also display large variation of Sm values. Thus, all the samples examined in this study are plotted between the spinel lherzolite melting trend and the garnet-lherzolite curve,

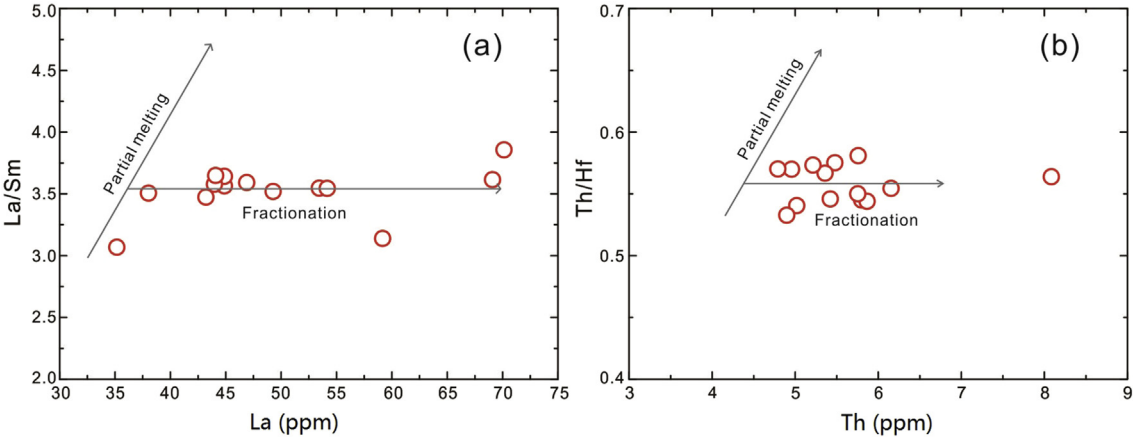

Figure 12. Plots of (a) La/Sm versus La and (b) Th/Hf versus Th for mafic dykes in the Helanshan showing theoretical correlation curves during fractional crystallization and partial melting (after Allegre and Minster, 1978).

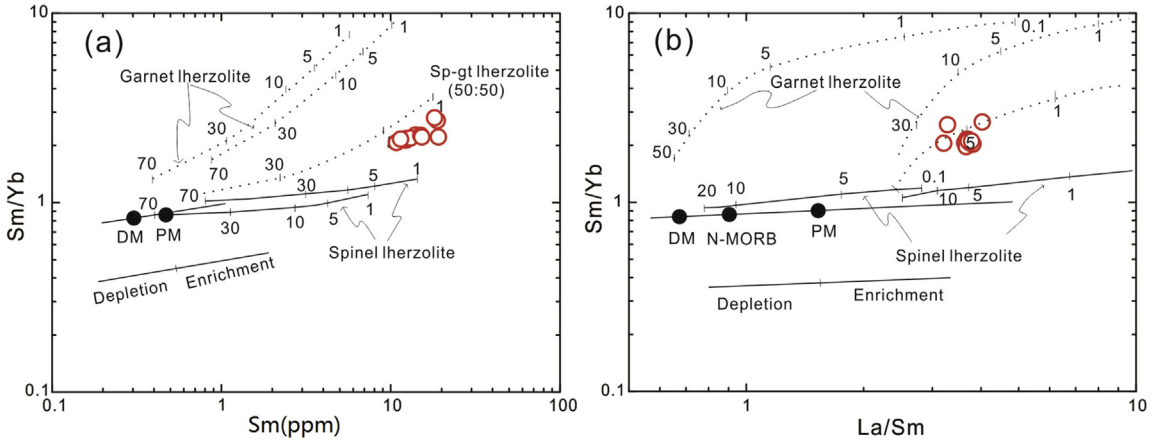

Figure 13. Plots of (a) Sm/Yb vs. Sm and (b) Sm/Yb vs. La/Sm for the mafic dykes in the Helanshan. The basic diagrams are after Zhao and Zhou (2006), and numbers along lines represent the degree of the partial melting.

and they fall near the garnet + spinel lherzolite curve in the Sm/Yb vs. Sm and Sm/Yb vs. La/Sm diagrams showing about 5% partial melting (Fig. 13a, b). Accordingly, it is proposed that the mafic dykes crystallized from melts formed by about 5% partial melting of a garnet + spinel lherzolite mantle source.

6.3. Tectonic setting and implications

The Late Triassic tectonic setting in the HTB has been debated with various models including collisional (Li et al., 1995; Chen, 1999; Jia et al., 2003, 2005; Ge et al., 2009; Yang et al., 2014; Yuan and Yang, 2015a,b), extensional rift (Liu, 1998; Ritts et al., 2004; Wang et al., 2005, 2006; Yang et al., 2010; Liu et al., 2013) and strike-slip tectonic settings (Zhang et al., 2009). Our data from the mafic dykes display relatively high TiO_2, Nb and Ta contents which are obviously different from those of volcanic arc basalts in a subduction and collisional setting (Pearce, 1982). The LREE enrichment displayed in the chondrite-normalized REE patterns, enrichment in incompatible elements (Fig. 11a) and lack of obvious Nb–Ta depletion in the primitive mantle-normalized trace element patterns (Fig. 11b) are typical characteristics of intra-plate basalts, and are different from those of magma derived from subduction-related volcanic arc setting. Moreover, the samples are enriched in Zr as compared to Y with the Zr/Y ratios (5.79–6.66), which are significantly higher than those of arc related basalts.

Although mafic dykes are commonly regarded as important indicators for extensional setting (Halls and Fahrin, 1987; Gudmunsson, 1995; Hou et al., 2006; Hou, 2012), their high REE contents, strong enrichment of LREE, and enrichment of LILE and HFSE, as well as they intruded into the basement rocks, these characteristics have also argued against an oceanic basin setting for the mafic dykes in the HTB. This is also indicated by their high Zr contents and Zr/Y ratios which suggest a within-plate setting for the mafic dykes (Fig. 14a). Although the covariant relations of $MgO–FeO^T–Al_2O_3$ (Fig. 14b) suggest a continental rift setting for the studied mafic dykes, their low SiO_2, ($K_2O + Na_2O$) contents and high-Fe tholeiite series (Fig. 8), together with lack of correlated rhyolitic rocks, precluded an interpretation of a rift setting.

Based on the above features, together with the fact that the dykes intruded into the basement rocks of the Helanshan Complex, it is reasonable to infer that the mafic dykes in the basement of the HTB were probably generated from mantle upwelling correlated to lithosphere extension and thinning. Further to the north, the Paleo-Asian Ocean closed during the Late Permian to Early Triassic (Xiao

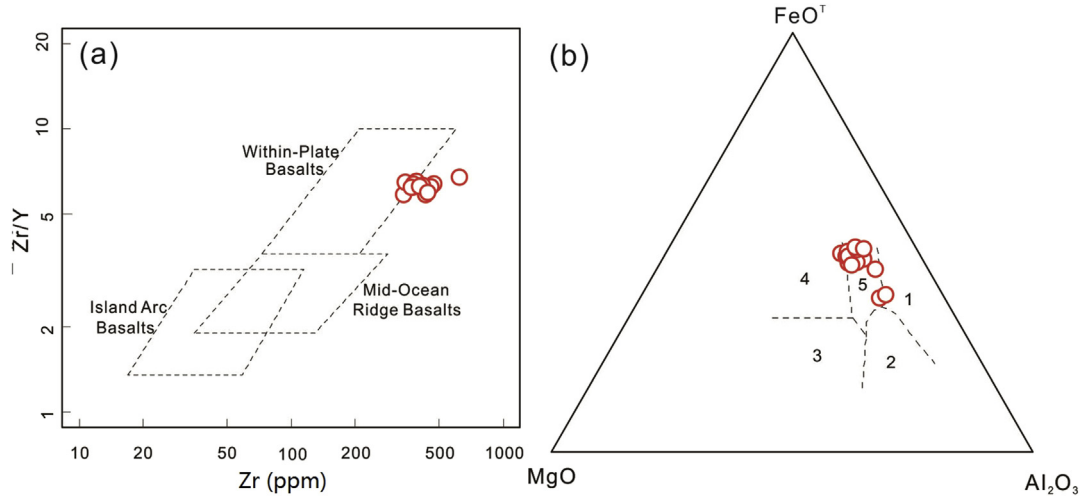

Figure 14. Discrimination diagrams for the mafic dykes in the Helanshan: (a) Zr/Y vs. Zr (Pearce and Norry, 1979) and (b) FMA (Condie et al., 1987). 1–Ice Island; 2–Orogen; 3–Mid-Ocean Ridge; 4–Ocean Island; 5–Continental Rift.

et al., 2010). The lithospheric extension and thinning suggested in our study is most likely related to the post-collisional collapse of the Central-Asian Orogen. The thinning and extension associated with post-collisional collapse has resulted in the partial melting of the lithospheric mantle, resulting in mafic magma upwelling and intruding into the crustal basement.

The Rujigou basalts most likely represent the contemporaneous heterotopic facies eruptions of the mafic magma. The outcrop of the basalts is 8 km in length and 0.2–0.5 km in width (Fig. 2). The basalts are conformably distributed in the Upper Triassic Yanchang Formation and are overlain by the middle Jurassic Yanan Formation with gentle angular unconformity (Wang et al., 2005). The basalt yielded a whole rock K–Ar age of 229 ± 15 Ma (BGMRNXHAR, 1990), which is broadly similar to the age (205.5 ± 1.9 Ma) of the mafic dyke in this study, as the whole rock K–Ar ages are usually older than the magmatic zircon ages because of excess argon (Aldrich and Nier, 1948; Li et al., 1999; Mcdougall, 2013). The Rujigou Basalts in the HTB are characterized by low potassic high-Fe tholeiite series. Their major and trace element signatures (BGMRNXHAR, 1990; Gao et al., 2003; Wang et al., 2005; Yang et al., 2010) are markedly similar to those of the mafic dykes in this study, and thus they are inferred to have the same origin as that of the Helanshan mafic dykes. Therefore, we proposed that the mafic dykes and the Rujigou basalts in the HTB are contemporaneous facies intrusions and eruptions of the mafic magma, generated within an extensional lithospheric setting. The lithosphere extension is also evidenced by the sedimentation in the Late Triassic, which is composed mostly of fluvial and lacustrine strata defining an extensional basin along the northwest margin of the Ordos basin (Liu, 1998; Ritts et al., 2004).

7. Conclusions

Geochronological and geochemical studies of the mafic dykes in the HTB lead to the following conclusions.

(1) The mafic dykes yield a LA-ICP-MS zircon U–Pb age of 205.5 ± 1.9 Ma, which represents their crystallization age.
(2) Elemental geochemistry indicates that they were derived from partial melting of an enriched, lithospheric mantle source. The magma of the dykes might have undergone significant crystal fractionation of olivine, pyroxene and plagioclase with minor crustal contamination.
(3) The mafic dykes intruded in an intracontinental extensional setting related to the post-collisional collapse of the Central Asian Orogen during the Late Triassic. Together with contemporaneous basalts in the HTB and sedimentation in the western Ordos basin, the HTB is considered to have undergone a significant thinning and extension event in the Late Triassic time.

Acknowledgments

Financial support for this study was jointly provided by the National Natural Science Foundation of China (Grant Nos. 41421002 and 41225008), MOST Special Fund from the State Key Laboratory of Continental Dynamics, Northwest University, and Project for Key Innovative Research Team of Science and Technology in Shaanxi Province (Grant No. 2013KCT-18).

Appendix A. Supplementary data

Supplementary data related to this article can be found at https://doi.org/10.1016/j.gsf.2017.09.006.

References

Albarède, F., Scherer, E.E., Blichert-Toft, J., Rosing, M., Simionovici, A., Bizzarro, M., 2006. γ-ray irradiation in the early solar system and the conundrum of the ^{176}Lu decay constant. Geochimica et Cosmochimica Acta 70, 1261–1270.
Aldanmaz, E., Pearce, J.A., Thirlwall, M.F., Mitchell, J.G., 2000. Petrogenetic evolution of late Cenozoic, post-collision volcanism in western Anatolia, Turkey. Journal of Volcanology and Geothermal Research 102, 67–95.
Aldrich, L.T., Nier, A.O., 1948. Argon 40 in potassium minerals. Physical Review 74, 876–877.
Allegre, C.J., Minster, J.F., 1978. Quantitative models of trace element behavior in magmatic processes. Earth and Planetary Science Letters 38, 1–25.
Belousova, E.A., Griffin, W.L., O'Reilly, S., Fisher, N.I., 2002. Igneous zircon: trace element composition as an indicator of source rock type. Contributions to Mineralogy and Petrology 143, 602–622.
BlichertToft, J., Albarede, F., 1997. The Lu-Hf isotope geochemistry of chondrites and the evolution of the mantle-crust system. Earth and Planetary Science Letters 148, 243–258.
Bureau of Geological and Mineral Resources of Ningxia Hui Autonomous Region (BGMRNHAR), 1990. Regional Geology of Ningxia Hui Autonomous Region. Geological Publishing House, Beijing, pp. 1–443 (in Chinese with English abstract).
Chen, G., 1999. Terrigenous clastic composition and its tectonic feature in the Mesozoic of the Ordos basin. Acta Sedimentologica Sinica 17, 409–413 (in Chinese with English abstract).
Condie, K.C., Bobrow, D.J., Card, K.D., 1987. Geochemistry of Precambrian mafic dykes from the southern Superior Province of the Canadian Shield. Special Paper-Geological Association of Canada 34, 95–108.
Corfu, F., Hanchar, J.M., Hoskin, P.W., Kinny, P., 2003. Atlas of zircon textures. Reviews in Mineralogy and Geochemistry 53, 469–500.
Dan, W., Li, X.H., Guo, J.H., Liu, Y., Wang, X.C., 2012. Integrated in situ zircon U–Pb age and Hf–O isotopes for the Helanshan khondalites in North China Craton: juvenile crustal materials deposited in active or passive continental margin? Precambrian Research 222–223, 143–158.
Dan, W., Li, X.H., Wang, Q., Wang, X.C., Liu, Y., Wyman, D.A., 2014. Paleoproterozoic S-type granites in the Helanshan Complex, Khondalite Belt, North China Craton: implications for rapid sediment recycling during slab break-off. Precambrian Research 254, 59–72.
Dan, W., Li, X.H., Wang, Q., Wang, C., Wyman, D., Liu, Y., 2016. Phanerozoic amalgamation of the Alxa Block and North China Craton: evidence from Paleozoic granitoids, U–Pb geochronology and Sr–Nd–Pb–Hf–O isotope geochemistry. Gondwana Research 32, 105–121.
Deniel, C., 1998. Geochemical and isotopic (Sr, Nd, Pb) evidence for plume-lithosphere interactions in the genesis of Grande Comore magmas (Indian Ocean). Chemical Geology 144, 281–303.
Ding, H.J., Meng, X.H., Ge, M., Xu, H.Y., 2009. Ordovician contourite of the north part of Helan Aulacogen. Journal of Earth Sciences and Environment 31, 58–64 (in Chinese with English abstract).
Dong, C.Y., Liu, D.Y., Li, J.J., Wan, Y.S., Zhou, H.Y., Li, C.D., Yang, Y.H., Xie, L.W., 2007. Palaeoproterozoic Khondalite Belt in the western North China Craton: new evidence from SHRIMP dating and Hf isotopic composition of zircons from metamorphic rocks in the Bayan UL-HeLan Mountains area. Chinese Science Bulletin 52, 2984–2994.
Dong, Y.P., Sun, S.S., Yang, Z., Liu, X.M., Zhang, F.F., Li, W., Cheng, B., He, D.F., Zhang, G.W., 2017. Neoproterozoic subduction-accretionary tectonics of the South Qinling Belt, China. Precambrian Research 293, 73–90.
Fitton, J.G., 1995. Coupled molybdenum and niobium depletion in continental basalts. Earth and Planetary Science Letters 136, 715–721.
Gao, S.L., Li, F., Li, T.B., Lu, C.G., Lu, Y.J., 2003. Discussion of the relationship between coal metamorphism and the Late Mesozoic basalt in Rujigou Area. Coal Geology and Exploration 31, 8–10 (in Chinese with English abstract).
Ge, X.H., Ma, W.P., Liu, J.L., Ren, S.M., Liu, Y.L., Yuan, S.H., Wang, M.P., 2009. A discussion on the tectonic framework of Chinese mainland. Geology in China 36, 949–965 (in Chinese with English abstract).
Geng, Y.S., Zhou, X.W., Wang, X.S., Ren, L.D., 2009. Late-Paleoproterozoic granite events and their geological significance in Helanshan area, Inner Mongolia: evidence from geochronology. Acta Petrologica Sinica 25, 1830–1842 (in Chinese with English abstract).
Gong, J.H., Zhang, J.X., Wang, Z.Q., Yu, S.Y., Li, H.K., Li, Y.S., 2016. Origin of the Alxa Block, western China: new evidence from zircon U–Pb geochronology and Hf isotopes of the Longshoushan Complex. Gondwana Research 36, 359–375.
Griffin, W.L., Pearson, N.J., Belousova, E., Jackson, S.E., van Achterbergh, E., O'Reilly, S.Y., Shee, S.R., 2000. The Hf isotope composition of cratonic mantle: LAM-MC-ICP–MS analysis of zircon megacrysts in kimberlites. Geochimica Et Cosmochimica Acta 64, 133–147.
Griffin, W.L., Pearson, N.J., Belousova, E.A., Saeed, A., 2006. Comment: Hf-isotope heterogeneity in zircon 91500. Chemical Geology 233, 358–363.
Gudmunsson, A., 1995. Infrastructure and mechanics of volcanic systems in Iceland. Journal of Volcanology and Geothermal Research 64, 1–22.
Halls, H.C., Fahrin, W.F., 1987. Mafic Dyke Swarms, pp. 1–10. Geological Association of Canada Special Paper 34.
Hou, G.T., Wang, C.H., Li, J.H., Qian, X.L., 2006. Late Paleoproterozoic extension and a paleostress field reconstruction of the North China Craton. Tectonophysics 422, 89–98.

Hou, G.T., 2012. Mechanism for three types of mafic dyke swarms. Geoscience Frontiers 3, 217–223.
Huang, X.N., Zhang, J.S., Peng, P., Li, T.B., 2013. Structural deformation characteristics of the Paleoproterozoic crystalline basement in the northern segment of Helan Mountain and its regional tectonic implications. Acta Petrologica Sinica 29, 2353–2370 (in Chinese with English abstract).
Huo, F.C., Pan, X.S., You, G.L., 1989. Geology of Ningxia. Science Press, Beijing, pp. 1–256 (in Chinese).
Jensen, L.S., 1976. A New Cation Plot for Classifying Sub-alkaline Volcanic Rocks. Ontario Division Mines Miscellaneous Paper 66, 21 pp.
Jia, C.Z., Wei, G.Q., Li, B.L., Xiao, A.C., Ran, Q.G., 2003. Tectonic evolution of two-epoch foreland basins and its control for natural gas accumulation in China's mid-western areas. Acta Petrologica Sinica 24, 13–17 (in Chinese with English abstract).
Jia, C.Z., Song, Y., Wei, G.Q., Zhao, M.J., Liu, S.B., Li, B.L., 2005. Geological features and petroleum accumulation in the foreland basins in central and western China. Earth Science Frontiers 12, 3–13 (in Chinese with English abstract).
Kinny, P.D., Wijbrans, J.R., Froude, D.O., Williams, I.S., Compston, W., 1990. Age constrains on the geological evolution of the Narryer gneiss comples, Western Australia. Australian Journal of Earth Science 37, 51–69.
Le Bas, M.J., Le Maitre, R.W., Streckeisen, A., Zanettin, B., 1986. A chemical classification of volcanic rocks based on the total alkali-silica diagram. Journal of Petrology 27, 745–750.
Li, D.M., Li, Q., Chen, W.J., 1999. Excess argon in plagioclase phenocryst of Tengchong volcanics and the related volcano erupting stages. Geological Review 45, 892–894.
Li, J.Y., Zhang, J., Qiu, J.F., 2012. Amalgamation of North China Craton with Alxa Block in the late of Early Paleozoic: evidence from sedimentary sequences in the Niushou Mountain, Ningxia Hui Autonomous Region, NW China. Geological Review 58, 208–214 (in Chinese with English abstract).
Li, Z.H., Liu, X.M., Dong, Y.P., Xiao, Z.B., 2013. Geochemistry and zircon U–Pb age of the Paleoproterozoic syn-collisional granites in Helanshan region and its geological significance. Acta Petrologica Sinica 29, 2405–2415 (in Chinese with English abstract).
Li, S.T., Yang, S.G., Tom, J., 1995. Upper Triassic-Jurassic foreland sequences of the Ordos basin in China. Society for Sedimentary Geology 52, 233–241.
Lin, C.S., Yang, Q., Li, S.T., 1995. The Analysis on the Filling and Evolution of the Helan Aulacogen. Geological Publishing House, Beijing, pp. 1–143 (in Chinese with English abstract).
Liu, S., Hu, R.Z., Gao, S., Feng, C.X., Qi, L., Zhong, H., Xiao, T.F., Qi, Y.Q., Wang, T., Coulson, L.M., 2008. Zircon U–Pb geochronology and major, trace elemental and Sr-Nd-Pb isotopic geochemistry of mafic dykes in western Shandong Province, east China: constrains on their petrogenesis and geodynamic significance. Chemical Geology 255, 329–345.
Liu, S., Hu, R.Z., Gao, S., Feng, C.X., Yu, B.B., Feng, G.Y., Qi, Y.Q., Wang, T., Coulson, L.M., 2009. Petrogenesis of Late Mesozoic mafic dykes in the Jiaodong Peninsula, eastern North China Craton and implications for the foundering of lower crust. Lithos 113, 612–639.
Liu, S.F., 1998. The coupling mechanism of basin and orogen in the western Ordos Basin and adjacent regions of China. Journal of Asian Earth Sciences 16, 369–383.
Liu, S.F., Su, S., Zhang, G.W., 2013. Early Mesozoic basin development in North China: indications of cratonic deformation. Journal of Asian Earth Sciences 62, 221–236.
Liu, X.M., Gao, S., Diwu, C.R., Yuan, H.L., Hu, Z.C., 2007. Simultaneous in-situ determination of U–Pb age and trace elements in zircon by LA-ICP-MS in 20 μm spot size. Chinese Science Bulletin 52, 1257–1264.
Liu, Y., Diwu, C.R., Zhao, Y., Liu, X.M., Yuan, H.L., Wang, J.Q., 2014. Determination of trace and rare-earth elements in Chinese soil and clay reference materials by ICP-MS. Chinese Journal of Geochemistry 33, 95–102.
Lu, L.Z., Xu, X.C., Liu, F.L., 1996. Early Precambrian Khondalite series of North China. Changchun Publishing House, Changchun, pp. 1–272 (in Chinese).
Ludwig, K.R., 2003. User's Manual for Isoplot/Ex. Version 3.00. A Geochronological Toolkit for Microsoft Excel. In: Berkeley Geochronology Center Special Publication, vol. 4.
Mcdougall, I., 2013. K/Ar and $^{40}Ar/^{39}Ar$ isotopic dating techniques as applied to young volcanic rocks, particularly those associated with hominin localities. Treatise on Geochemistry 14, 1–15.
Pearce, J., Norry, M., 1979. Petrogenetic implications of Ti, Zr, Y, and Nb variations in volcanic rocks. Contributions to Mineralogy and Petrology 69, 33–47.
Pearce, J.A., 1982. Trace element characteristics of lavas from destructive plate boundaries. In: Thorpe, R.S. (Ed.), Andesites: Orogenic Andesites and Related Rocks. Wiley, Chichester, pp. 525–548.
Ritts, B.D., Hanson, A.D., Darby, B.J., Nanson, L., Berry, A., 2004. Sedimentary record of Triassic intraplate extension in North China: evidence from the nonmarine NW Ordos Basin, Helan Shan and Zhuozi Shan. Tectonophysics 386, 177–202.
Rudnick, R.L., Gao, S., 2003. Composition of the continental crust. In: Heinrich, D.H., Karl, K.T. (Eds.), Treatise on Geochemistry. Pergamon, Oxford, pp. 1–64.
Schiøtte, L., Compston, W., Bridgwater, D., 1988. Late Archaean ages for the deposition of clastic sediments belonging to the Malene supracrustal, southern West Greenland: evidence from an ion probe U-Pb zircon study. Earth and Planetary Science Letters 87, 45–58.
Sun, S.S., McDonough, W.F., 1989. Chemical and isotopic systematics of oceanic basalts: implications for mantle composition and processes, magmatism in the Ocean Basins. In: Geological Society of London, Special Publications, vol. 42, pp. 313–345.
Wang, F., Liu, C.Y., Yang, X.K., Su, C.Q., 2005. Geologic geochemical features of Basalt in Ruqi Clough of Helan Mountain and its structural environmental significance. Petroleum Geology and Oilfield Development in Daqing 24 (4), 25–27 (in Chinese with English abstract).
Wang, F., Liu, C.Y., Zhao, H.G., Yang, X.K., Su, C.Q., 2006. Relationship between Helanshan Basin and Ordos Basin. Acta Petrolei Sinica 27 (4), 15–22 (in Chinese with English abstract).
Wang, Z.T., Zhou, H.R., Wang, X.L., Zheng, M.P., Santosh, M., Jing, X.C., Zhang, J., Zhang, Y.S., 2016. Detrital zircon fingerprints link western North China Craton with East Gondwana during Ordovician. Gondwana Research 40, 58–76.
Wiedenbeck, M., Hanchar, J.M., Peck, W.H., Sylvester, P., Valley, J., Whitehouse, M., Kronz, A., Morishita, Y., Nasdala, L., Fiebig, J., Franchi, I., Girard, J.P., Greenwood, R.C., Hinton, R., Kita, N., Mason, P.R.D., Norman, M., Ogasawara, M., Piccoli, P.M., Rhede, D., Satoh, H., Schulz-Dobrick, B., Skår, Ø., Spicuzza, M.J., Terada, K., Tindle, A., Togashi, S., Vennemann, T., Xie, Q., Zheng, Y.F., 2004. Further characterisation of the 91500 zircon crystal. Geostandards and Geoanalytical Research 28, 9–39.
Williams, I.S., Claesson, S., 1987. Isotopic evidence for the Precambrian provenance and Caledonian metamorphism of high grade paragneisses from the Seve Nappes, Scandinavian Caledonides. Contributions to Mineralogy and Petrology 97, 205–217.
Winchester, J.A., Floyd, P.A., 1977. Geochemical discrimination of different magma series and their differentiation products using immobile elements. Chemical Geology 20, 325–344.
Wu, Y.B., Zheng, Y.F., 2004. Genesis of zircon and its constraints on interpretation of U–Pb age. Chinese Science Bulletin 49, 1554–1569.
Xiao, P.X., You, W.F., Xie, C.R., Li, P., Bai, S.M., 2011. LA-ICP-MS U–Pb detrital zircon geochronology of alumina-rich gneiss of the Helanshan complex-group in the northern segment of Helanshan and regional comparison. Geological Bulletin of China 30, 26–36 (in Chinese with English abstract).
Xiao, W.J., Mao, Q.G., Windley, B.F., Han, C.M., Qu, J.F., Zhang, J.E., Ao, S.J., Guo, Q.Q., Cleven, N.R., Lin, S.F., Shan, Y.H., Li, J.L., 2010. Paleozoic multiple accretionary and collisional processes of the Beishan Orogenic collage. American Journal of Science 310, 1553–1594.
Xu, S.M., Feng, H.W., Li, S.Z., Li, M., Ian, S., Bi, H.M., Ji, Y., Ye, Q., 2015. Closure time in the East Qilian Ocean and Early Paleozoic ocean-continent configuration in the Helan Mountains and adjacent regions, NW China. Journal of Asian Earth Sciences 113, 575–588.
Yang, H., Fu, J.H., Ouyang, Z.J., Liu, S.Y., Ma, Z.R., 2010. U–Pb zircon dating of the Daling-Gugutai Basalt in Rujigou on the Western Margin of Ordos Basin. Acta Geoscientics Sinica 31, 229–236 (in Chinese with English abstract).
Yang, Z.Y., Yuan, W., Tong, Y.B., Liu, J., Wang, Y., 2014. Tectonic affinity reconnaissance of the Alxa Block in the Pre-Mesozoic. Acta Geoscientics Sinica 35, 673–681 (in Chinese with English abstract).
Yin, C.Q., Zhao, G.C., Guo, J.H., Sun, M., Xia, X.P., Zhou, X.W., Liu, C.H., 2011. U–Pb and Hf isotopic study of zircons of the Helanshan Complex: constrains on the evolution of the Khondalite Belt in the Western Block of the North China Craton. Lithos 122, 25–38.
Yuan, H.L., Gao, S., Dai, M.N., Zong, C.L., Günther, D., Fontaine, G.H., Liu, X.M., Diwu, C.R., 2008. Simultaneous determinations of U-Pb age, Hf isotopes and trace element compositions of zircon by excimer laser-ablation quadrupole and multiple-collector ICP-MS. Chemical Geology 247, 100–118.
Yuan, W., Yang, Z.Y., 2012. The affinity of the Hexi Corridor and Australia – evidence from U–Pb geochronology and Hf isotopes of detrital zircons from Middle Cambrian strata in Niushoushan. Geological Bulletin of China 31, 1537–1553 (in Chinese with English abstract).
Yuan, W., Yang, Z.Y., 2015a. The Alashan Terrane was not part of North China by the late Devonian: evidence from detrital zircon U–Pb geochronology and Hf isotopes. Gondwana Research 27, 1270–1282.
Yuan, W., Yang, Z.Y., 2015b. The Alashan Terrane did not amalgamate with North China block by the Late Permian: evidence from carboniferous and Permian paleomagnetic results. Journal of Asian Earth Sciences 104, 145–159.
Zhang, K., 1989. Tectonics and Recourses of Ordos Fault Block. Shanxi Science and Technology Press, Xi'an, pp. 1–394 (in Chinese).
Zhang, J., Ma, Z.J., Ren, W.J., 2004. Re-discussion on natures of extension in Helanshan region before Cenozoic era. Acta Petrologica Sinica 25, 8–11 (in Chinese with English abstract).
Zhang, J., Li, J.Y., Ma, Z.J., Ren, W.J., 2009. The tectonic setting of the Triassic Basin in the Helanshan Mts. Acta Geologica Sinica 83, 1233–1246 (in Chinese with English abstract).
Zhang, J., Li, J.Y., Liu, J.F., Feng, Q.W., 2011. Detrital zircon U–Pb ages of Middle Ordovician flysch sandstones in the western ordos margin: new constraints on their provenances, and tectonic implications. Journal of Asian Earth Sciences 42, 1030–1047.
Zhang, J., Li, J.Y., Liu, J.F., Li, Y.F., Qu, J.F., Feng, Q.W., 2012. The relationship between the Alxa Block and the North China plate during the Early Paleozoic: new information from the Middle Ordovician detrial zircon ages in the eastern Alxa Block. Acta Petrologica Sinica 28, 2912–2934 (in Chinese with English abstract).
Zhang, J., Zhang, Y.P., Xiao, W.X., Wang, Y.N., Zhang, B.H., 2015. Linking the Alxa Terrane to the eastern Gondwana during the Early Paleozoic: constraints from detrital zircon U–Pb ages and Cambrian sedimentary records. Gondwana Research 28, 1168–1182.

Zhang, J., Zhang, B.H., Zhao, H., 2016. Timing of amalgamation of the Alxa Block and the North China Block: constraints based on detrital zircon U–Pb ages and sedimentologic and structural evidence. Tectonophysics 668, 65–81.

Zhao, G.C., Sun, M., Wilde, S.A., Li, S.Z., 2005. Late Archean to Paleoproterozoic evolution of the North China Craton: key issues revisited. Precambrian Research 136, 177–202.

Zhao, G.C., 2009. Metamorphic evolution of major tectonic units in the basement of the North China Craton: key issues and discussion. Acta Petrologica Sinica 25, 1772–1792 (in Chinese with English abstract).

Zhao, G.C., Wilde, S.A., Guo, J.H., Cawood, P.A., Sun, M., Li, X.P., 2010. Single zircon grains record two Paleoproterozoic collisional events in the North China Craton. Precambrian Research 177, 266–276.

Zhao, G.C., Zhai, M.G., 2013. Lithotectonic elements of Precambrian basement in the North China Craton: review and tectonic implications. Gondwana Research 23, 1207–1240.

Zhao, J.H., Zhou, M.F., 2006. Neoproterozoic mafic intrusions in the Panzhihua district, SW China: implications for interaction between subducted slab and mantle wedge. Geochimica et Cosmochimica Acta 70, A740–A1740.

Zhao, J.H., Zhou, M.F., 2007. Geochemistry of Neoproterozoic mafic intrusions in the Panzhihua district (Sichuan Province, SW China): implications for subduction-related metasomatism in the upper mantle. Precambrian Research 152, 27–47.

Zhou, X.W., Zhao, G.C., Geng, Y.S., 2010. Helanshan high pressure pelitic granulite Petrologic evidence for collision event in the western block of the North China Craton. Acta Petrologica Sinica 26, 2113–2121 (in Chinese with English abstract).